



Present and future projections of heatwave hazard-risk over India: A regional earth system model assessment



Aditya Kumar Dubey ^a, Preet Lal ^{a,b}, Pankaj Kumar ^{a,*}, Amit Kumar ^b, Anton Y. Dvornikov ^c

^a Department of Earth and Environmental Sciences, Indian Institute of Science Education and Research Bhopal, India

^b Department of Geoinformatics, Central University of Jharkhand, Ranchi, India

^c Shirshov Institute of Oceanology, Russian Academy of Sciences, Moscow, Russia

ARTICLE INFO

ABSTRACT

Keywords:

Heatwave hazards
Vulnerability
Risk
Projection
Regional earth system model

The heatwave is a disastrous hazard having significant impacts on health and society. This study analyses the heatwave hazards and risk for India's current and future scenarios using socioeconomic vulnerability and temperature datasets during the summer (April–June) season. The Census of India (CoI) 2011 datasets were considered to assess current vulnerability and projected from the SocioEconomic Data And Application Center (SEDAC) population at Shared Socioeconomic Pathway (SSP) 4 for future vulnerability. Whereas IMD temperature data used for hazard assessment for the present scenario (1958–2005) while projected temperature data from regional earth system model REMO-OASIS-MPIOM (ROM) were used for the future (2006–2099) scenario. The study exhibited the most hazardous, vulnerable, and risk-prone regions identified as the south-eastern coast and Indo-Gangetic plains and some populous districts with metropolitan regions (Mumbai, Delhi, and Kolkata) under the current scenario. The coupled model ROM has efficiently captured the critical districts with higher and lower risk, showing its future projection capability. The study highlighted that the heatwave hazard-risk would significantly worsen in future scenarios in all districts under enhanced global warming and largely affecting the districts in the eastern and middle Indo-Gangetic plains and Malabar region. The present study will provide sufficient insights into designing mitigation strategies and future adaptive planning for the heatwave risk, which is one of the targets under Sustainable Development Goal 13 (Goal 13: Climate Action).

1. Introduction

Heatwaves pose an evolving natural hazard of excessive heat, whose intensity, frequency, and duration are increasing due to the combined impacts of the warming climate and escalated anthropogenic influences in the recent decades (Perkins and Alexander, 2013; Perkins-Kirkpatrick and Lewis, 2020). The heatwaves have affected not only humans but also other organisms and the economy. It has caused enormous loss of human lives worldwide, such as Europe's heatwave in 2003, which killed approx. 77,000 people (Robine et al., 2008), Russia, in 2010, killed ~55,000 people (Barriopedro et al., 2011; Otto et al., 2012). The risk due to heatwave disasters is one of the greatest threats to humans, which will rise further with the increase in temperature as projected to ~3–6 °C at the end of the century (IPCC, 2014). Considering its vast implications, the heatwave is one of the major variables cited in the Sustainable

Development Goals (SDG) under goal 13 (climate action), which aims to limit global warming to 1.5 °C and related threats due to heat extremes. Since it is already reported that the frequency, duration, and intensity of such events are expected to increase (IPCC, 2014; Mukherjee and Mishra, 2018; Rohini et al., 2019), it is essential to develop appropriate tools for identifying hazardous regions and associated risks to assess potential impacts on human health (Meehl and Tebaldi, 2004). According to the Intergovernmental Panel on Climate Change (IPCC, 2014), climate change risks are determined by climate extremes (the hazards) and society's exposure and vulnerability to these hazards. Though the SDG 13 limits the use of coals and other greenhouse gas emitters, the temperature increase is not yet under control. Therefore, the heatwave risk projection will help to identify the highest risk-prone zones and develop mitigation strategies. Also, one of the targets of SDG 13 is to strengthen resilience and improve the mitigation strategies due to climate-related

* Corresponding author. Department of Earth and Environmental Sciences, Indian Institute of Science Education and Research Bhopal, Bhopal-Indore by-pass, Bhopal, India.

E-mail addresses: adityadubey@iiserb.ac.in (A.K. Dubey), preetlal2011@gmail.com (P. Lal), kumarp@iiserb.ac.in (P. Kumar), amit.kumar@cuj.ac.in (A. Kumar), anton.dvornikoff@gmail.com (A.Y. Dvornikov).

hazards, including heatwave. Being located in the tropical and subtropical region, India is among the world's most hazardous prone countries towards heatwave. Previously, some of the most devastating heat waves were evident in 1998, 2010, and 2015, which caused considerable loss of thousands of lives (Azhar et al., 2014; Pattanaik et al., 2017) and affected human health, agricultural practices, and infrastructures. The frequency and intensity of heatwave events in India have increased during the previous decades and are projected to increase in the future (Kumar et al., 2013; Rohini et al., 2019).

There is no such universal index for a heatwave, which can be applied across the globe (Robinson, 2001; Smith et al., 2013) as it varies from region to region based on regional thresholds or defined by the respective countries' met offices. However, the World Meteorological Organisation (WMO) has defined some indexes, which can be applied to the region through some modifications based on regional climate. The heatwave definitions are either based on absolute or percentile threshold when the only temperature is used (Robinson, 2001). It may be combined with humidity or/and wind to define a combined index that provides a better measure but will only be applicable in the region having such climatic conditions. Indian Meteorological Department has defined heatwaves based on climatological threshold and deviation from it, including the absolute thresholds for the hilly and plain regions. However, various studies have used the percentile threshold for defining heatwaves over India (Rohini et al., 2016; Mukherjee and Mishra, 2018; Dubey et al., 2021; Sharma et al., 2018).

Heatwaves pose a significant threat to the existing population by affecting their comfort levels and even leading to the loss of lives. The risk due to heatwave hazards is vital as it silently impacts our society (Perkins and Alexander, 2013). It depends on the socioeconomic status of the population, gender, age, as well as exposure and vulnerability of the population from the heatwave hazard. Densely populated areas are at more risk than sparsely populated areas (Buscail et al., 2012). The existing medical conditions (comorbidity), such as heart diseases, cardiovascular and respiratory diseases, renal diseases, exacerbate the fatality during the heatwave (Basarin et al., 2020). Populations residing alone irrespective of their age are at more health risk (Buscail et al., 2012; Klinenberg, 2003). The heatwave risk also depends on the type of structure where a person resides. For example, urban buildings are warmer than rural ones causing increased heatwave risk than rural ones (Clarke, 1972). However, other factors such as access to cooling machines (air condition) can reduce the risk in urban areas. Therefore, the future risk will depend on the demographic structure, including age, gender ratio, technological advancement, and economic growth. Better technology and adaptation measures may reduce the effect of such a hazard. It is arduous to project future age structure, income, male-female ratio, etc., but the future population and its density are projected based on various assumptions (Gao, 2020).

The global or regional climate models (GCMs) or Regional Climate Models (RCMs) are vital tools for understanding the present and future climate, including extremes (Giorgi et al., 2014). GCMs can simulate large-scale features, but they have difficulty simulating small-scale processes and extreme events (Dosio, 2016). However, RCMs are more efficient in simulating local scale features, including extremes (*viz.*, heatwaves) due to higher horizontal resolution and includes regional parameterizations (Diffenbaugh et al., 2005; Mishra and Dwivedi, 2019; Mishra et al., 2020a,b). The future projections of a heatwave over India have been made using global climate models (Coupled Model Inter-comparison Project Phase 5 CMIP5) and stand-alone regional climate models (Regional Climate Model Intercomparison Project) in various studies (Murari et al., 2015; Im et al., 2017; Mishra et al., 2017; Rohini et al., 2019; Singh et al., 2020). Regional earth system models (RESMs) are the best tools to study the regional phenomenon and extremes due to higher resolution and dynamical air-sea interaction. (Mishra et al., 2021a; Ratnam et al., 2009). Coupled models are more efficient than stand-alone RCMS in simulating regional features due to the air-sea coupling from the ocean to the atmosphere and vice-versa

(Ratnam et al., 2009; Samala et al., 2013; Zou and Zhou, 2013; Mishra et al., 2021a). So far, none of the studies has used either GCMs, RCMs, or RESMs for India's heatwave hazard and risk analysis. Therefore, we performed an analysis of validation and projections of heatwave risk and vulnerability for India using a coupled regional ocean-atmosphere model ROM, which is the first attempt of its kind. The heatwave hazard and risk are compared against observation along with future projections up to the end of this century. Future changes in vulnerability and risk were analyzed using ROM with the forcing from the highest representative concentration pathway (RCP 8.5) emission scenario.

2. Data and methods

2.1. Data

The daily gridded mean maximum (T_{\max}) surface air temperature data were obtained from the Indian Meteorological Department (IMD) for 1951–2019 at $1^{\circ} \times 1^{\circ}$ horizontal resolution (Srivastava et al., 2009). This data was prepared using quality-controlled temperature datasets from 395 stations applying shepherd's angular distance weighting interpolation method. This data is useful for validations and studying the extreme events, including heatwave, and have been previously used in various studies for the same (Ratnam et al., 2016; Rohini et al., 2016; Singh et al., 2020).

2.1.1. Demographic and socioeconomic data

Demographic and socioeconomic datasets for India at the district level were obtained from the Census of India (CoI) 2011. Various contributing demographic variables (such as gender, age, education, caste, occupation, etc.) at the district level were used in the study (Table S1).

Future gridded population demographic dataset was acquired from Socio-Economic Data And Application Center (SEDAC) at a horizontal resolution of 1×1 km and at each decadal time-scale (Gao, 2017, 2020). These datasets are based on shared socioeconomic pathways (Riahi et al., 2017). We have used the Shared Socioeconomic Pathway 4 (SSP4) future projected population datasets for the years 2050, 2080, and 2100. It is the pathway that refers to the high inequalities with low mitigation challenges and high adaptive challenges (Calvin et al., 2017). The difference will increase in the future between wealthy and highly educated society and the poor and highly educated society (KC and Lutz, 2017).

2.1.2. Model description

The regional earth system model ROM consists of the REgional Atmosphere Model (REMO), the Max Planck Institute Ocean Model (MPIOM), the Hydrological Discharge model (HD), and the global marine biogeochemistry Hamburg Ocean Carbon Cycle model (HAMOCC). All models have been coupled via Ocean Atmosphere Sea Ice Soil (OASIS) coupler. The coupling frequency between the atmosphere and ocean is 3 h over the coupled region, whereas surface runoff and drainage from REMO to the HD and from HD to MPIOM occur daily (Sein et al., 2015; Mishra et al., 2021b). REMO is a hydrostatic regional atmosphere model used over the South-Asia CORDEX domain at $0.22^{\circ} \times 0.22^{\circ}$ (~ 25 km) horizontal resolution with 27 vertical atmospheric levels (Jacob et al., 2001). Fig. 1 shows the South-Asia CORDEX domain and orography of the ROM. The black polyline shows the India domain on which the study is conducted. The atmospheric component of ROM, whose dynamical core and space and time discretization are taken from the Europa model (Majewski, 1991). The physical parameterizations are used from the global climate model, ECHAM 4 and 5 (Roeckner et al., 1996, 2003). REMO has a rotated grid with an equator in the middle of the domain to avoid differences in the cell's size close to the poles. REMO uses horizontal discretization based on the Arakawa-C grid and hybrid vertical coordinates (Simmons and Burridge, 1981). REMO was simulated as a warm-start method that means soil temperature and soil

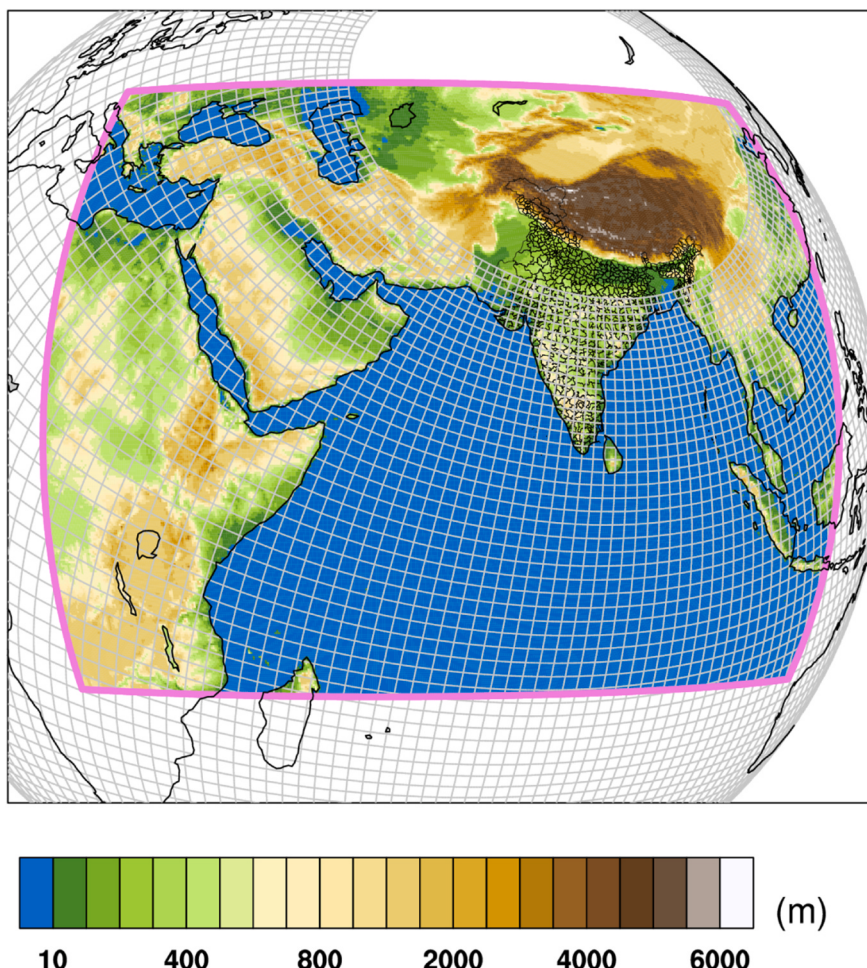


Fig. 1. The rectangle shows the coupled model domain set up. The grey lines show the grid of the MPIOM ocean/sea-ice model (only every 12th line is shown). The shaded colour scale represents orography (m). The black outline shows the Indian domain with district subdivisions, where the study is conducted. (For interpretation of the references to colour in this figure legend, the reader is referred to the Web version of this article.)

moisture variables were in a near-equilibrium state to limit their effect on surface parameters (Gao et al., 2015). More details about the model and its characteristics can be found from Jacob et al. (2001) and Sein et al. (2015).

MPIOM is the oceanic component of the coupled setup, a free surface primitive equation-based global model based on Boussinesq and incompressibility approximations (Marsland et al., 2003; Jungclaus et al., 2013). The advantage of having a global ocean domain is that it avoids complications related to the prescription of lateral boundary conditions (Sein et al., 2020). The grid configuration is an orthogonal curvilinear Arakawa C-grid with z-level vertical discretization (Arakawa and Lamb, 1977). This grid structure allows the placement of the poles over land, removing the numerical singularity associated with the convergence of meridians at the geographical North Pole (Sein et al., 2015). It also provides a choice of keeping high resolution over the desired region keeping global domain (Sein et al., 2015). The difficulties with open or closed boundaries in a regional ocean model is also solved using this grid structure. The horizontal resolution near the atmospheric domain, i.e., the Indian Ocean, is ~20 km, decreases up to 80 km as we move away from the Indian Ocean and reaches ~10 km near the coasts. The initial conditions for both atmosphere and ocean were obtained from previous spin-up simulations (50 years MPI-ESM stand-alone runs plus two times 40 years runs with coupled REMO/MPIOM simulations).

The third component of RESM is the HD model (Hagemann and Dümenil Gates, 2001; Hagemann et al., 2009), which runs on the global domain at a horizontal resolution of $0.5^\circ \times 0.5^\circ$ and daily temporal

resolution. The model details are briefly discussed in Hagemann and Dümenil Gates (2001). The fourth component of ROM is the HAMOCC model, which simulates the inorganic and organic biogeochemistry of water columns, and sediments and their exchange with the atmosphere and the ocean (Maier-Reimer, 1993; Maier-Reimer et al., 2005). It also simulates the nutrients, phytoplankton, detritus, and zooplankton cycles. More description about the HAMOCC is described in Sein et al. (2015). However, this component of ROM is switched off for the simulation used in this study.

The model was used for historical (1980–2005) and future (2006–2099) simulations using forcing from the global earth system model MPI-ESM-LR (Giorgetta et al., 2013). The MPI-ESM historical simulation was initialized from a preindustrial control run (PI-Control) and ran for the period 1920–2005 (historical) and 2006–2099 (future) in which the first thirty years is considered as an adjustment period. For future scenario runs, RCP8.5 emission pathway radiative forcing was used because it is the most promising scenario at which the present climate behaves (Wobus et al., 2018).

2.2. Methodology

2.2.1. Heatwave calculation

The definition of heatwave used in the study is adapted from the WMO Expert Team on Climate Change Detection Indices (Zhang et al., 2011). It is defined as the number of days above the 90th percentile value for consecutive six days or more for the base period. The analysis's

base period is taken as 1980–2005, and the 90th percentile is also calculated for the same period. The frequency is calculated as the average number of events following the above definition during the season. The days are counted consecutively six days or more, and the next event starts after completing this event. We have considered the AMJ season for heatwave calculation as the highest number of heatwaves occurs during this season (Singh et al., 2020).

Before proceeding towards calculating heatwave characteristics, IMD data was remapped to a horizontal resolution of $0.25^\circ \times 0.25^\circ$ using a bi-linear interpolation method to bring it to the model's resolution. The annual cycle was calculated for IMD and ROM data by area-averaging over India for the base period (1980–2005).

2.2.2. Vulnerability and risk calculation

Vulnerability refers to susceptibility to potential losses from hazard events of society's resistance and resilience to hazard (Bolin and Stanford, 1999). Various attributes of CoI demographic datasets have been used to calculate district-wise vulnerability across India. The district-scale CoI datasets were spatially joined with the thematic layer of district boundaries by matching the census code. All the datasets' units are dimensionless, so they are normalized between 1 and 10 scale as per vulnerability. The low value shows that districts are less vulnerable and vice-versa.

On the other hand, IPCC Third Assessment Report, AR3 (McCarthy et al., 2001) described the vulnerability as "a function of the character, magnitude, and rate of climate variation to which a system is exposed, its sensitivity, and its adaptive capacity". It defined vulnerability as "the degree to which a system is susceptible to or unable to cope with adverse effects of climate change, including climate variability and extremes", which is analogous to the definition of risk reported in the AR5 report. Vulnerability to impacts is a multi-dimensional concept encompassing bio-geophysical, economic, institutional and socio-cultural factors. Mathematically vulnerability is expressed (Turner et al., 2003):

$$\text{Vulnerability} = f(\text{Exposure}, \text{Sensitivity})$$

Exposure is a measure of the degree and nature to which any system or organism is exposed to any climatic variation. It can be interpreted as direct danger (stress) due to change in nature and severity of regional climate variables (e.g., extreme events) (Singh et al., 2014). Sensitivity is the degree to which an organism is affected either positively or negatively by any climatic event (Zhu et al., 2014). It describes the human-environmental conditions, which may worsen the hazard or can trigger the impact. Census data provides information about the spatial distribution of the required vulnerability characteristics at the district level.

Risk is the probability of an event with the consequences of an event

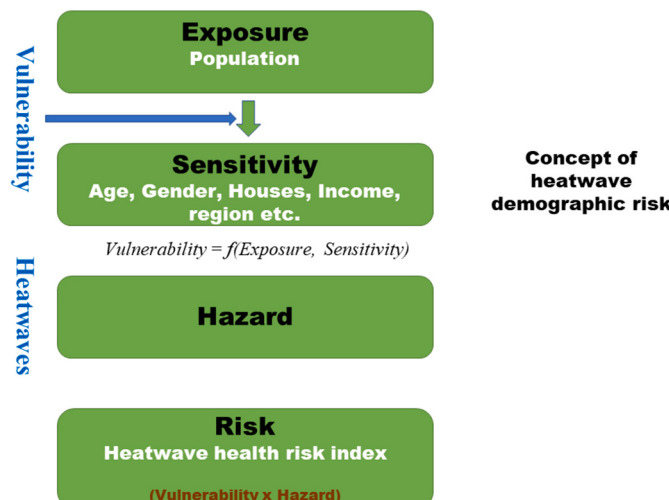


Fig. 2. Methodology flowchart for heatwaves risk mapping over India.

(IPCC, 2014) (Fig. 2):

$$\text{Risk (R)} = f(\text{Probability of a Hazard (H)} \times \text{Vulnerability (V)})$$

(equation-1)

To assess vulnerability, multi-criteria decision modelling (MCDA) has been used to avoid biases in weightage for different layers of demographic data. Among various methods in MCDA, the fuzzy analytical hierarchy process (F-AHP) has been used for weightage calculation. AHP is a scientific, pairwise comparison based multiple criteria decision-making (MCDM) method for decision-making to select the best potential alternatives (Saaty and Kearns, 2014). For obtaining a weightage or priority on various demographic data, it uses a pairwise comparison matrix and criteria are paired with a measurement scale. Still, it is having a factor of subjectivity in retrieving decisions. This method also takes into account data validity with inconsistency limits. The Fuzzy AHP method is similar to AHP but developed on fuzzy logic for priority decisions.

The analysis of fuzzy was considered in the following steps:

Let $X = \{x_1, x_2, x_3, \dots, x_n\}$ be a set of objects.

$U = \{u_1, u_2, u_3, \dots, u_n\}$ are aims.

Now each object has to undergo an extended analysis for all the problems. As a result, m will be obtained as follows:

$$M_{gi}^1, M_{gi}^2, \dots, M_{gi}^m \quad i = 1, 2, \dots, n$$

M_{gi}^j is the triangular fuzzy number.

It is the extent analysis values of the i th object for an m th aim, then the synthetic fuzzy value can be defined as:

$$S_i = \sum_{j=1}^m M_{gi}^j \odot \left[\sum_{i=1}^n \sum_{j=1}^m M_{gi}^j \right]^{-1}$$

Fuzzy AHP has 3 values for the evaluation of particular criteria, and arithmetic operations are required.

If there are two TFNs,

$$M_1 = (l_1, m_1, u_1) \text{ and } M_2 = (l_2, m_2, u_2)$$

$$(l_1, m_1, u_1) \oplus (l_2, m_2, u_2) = (l_1 + l_2, m_1 + m_2, u_1 + u_2)$$

$$(l_1, m_1, u_1) \odot (l_2, m_2, u_2) = (l_1 l_2, m_1 m_2, u_1 u_2)$$

$$(\lambda, \lambda, \lambda) \odot (l_2, m_2, u_2) = (\lambda l_2, \lambda m_2, \lambda u_2), \text{ for } \lambda > 0, \lambda \varepsilon(l_1, m_1, u_1)^{-1} = \left(\frac{1}{u_1}, \frac{1}{m_1}, \frac{1}{l_1} \right)$$

whereas λ = Fuzzy eigenvalue

The next step in fuzzy AHP includes the comparison of the degree of possibilities that $M_2 \geq M_1$. The comparison between two TFNs allows computing the degree of possibilities that $M_2 \geq M_1$ and $M_1 \geq M_2$. Thus $V(M_2 \geq M_1)$ expressed by:

$$V(M_2 \geq M_1) = \mu(h) = \begin{cases} 1, & \text{if } m_2 \geq m_1 \\ 0, & \text{if } l_1 \geq u_2 \\ \frac{l_1 - u_2}{(m_2 - u_2) - (m_1 - l_1)}, & \text{otherwise} \end{cases}$$

where "h" is ordinate of the highest intersection point between two membership functions.

Computation of smallest degree of possibilities ($M_2 \geq M_1$).

For comparing all the possible fuzzy values, $M_i = (1, 2, \dots, k)$ here minimum should be specified to compare all fuzzy values.

$$V(M \geq M_1, M_2, \dots, M_k) = \min V(M \geq M_1), i = 1, 2, \dots, n$$

Now calculating the weight vector for variants. The assumption to be made as:

$$h'(A_i) = V(S_i \geq S_k) \text{ for } k = 1, 2, \dots, n, i \neq k$$

The unnormalized weight vector is now represented as:

$$W' = (h'(A_1), h'(A_2), \dots, h'(A_n))^T$$

Now to calculate the priority weight vector for an individual object, one needs to apply normalizations:

$$W = (h(A_1), h(A_2), \dots, h(A_n))^T$$

where "W" is a crisp number and normalized vector.

Finally, an essential step to be applied in fuzzy AHP methodology for checking the consistency ratio of the pairwise comparison matrix. In fuzzy AHP, CR is preceded by the following defuzzification of matrix, and it is assumed that TFN $M = (l, m, u)$ transformed into a crisp number using the equation:

$$P(M) = \frac{l + 4m + u}{6}$$

After defuzzification, Satty's consistency is applied to the pairwise comparison matrix.

The present date vulnerability was calculated using CoI datasets. The criteria of providing weights to the demographic variables are based on how they can positively or negatively contribute to heatwave hazard impact. The weights assigned to these variables are tabulated in Table S1. Similarly, future vulnerability is calculated using the SEDAC dataset. For future SEDAC, population data is used for future vulnerability calculation as all the variables used from CoI are not available. Therefore, future projections are based solely on future hazards calculated using ROM simulated data and vulnerability, considering projected population data. The gridded SEDAC SSP-4 population data are converted into district-level data by using area-weighted mean. Now

district-scale population datasets normalized between 0 and 10 as per three different decade datasets and considered as higher the value more the vulnerability. The vulnerability datasets have been used to assess the risk for the future as per equation-1.

3. Results and discussion

3.1. Evaluation of maximum air temperature and its projection

The heatwave hazard estimation in this study is defined based on the region's daily maximum temperature (T_{\max}). To understand the model's efficiency, the temperature is compared with the IMD gridded observational data by using seasonal means of the considered period. The spatial patterns of T_{\max} are almost similar, except over the northern Himalayas and northeast regions (Fig. 3a and b). Fig. 3c shows the T_{\max} annual cycle of all India area-averaged IMD and ROM for the base period. ROM is able to simulate the annual cycle quite realistically, especially for the study season (AMJ), where observation and model are overlaid point to point. However, the model shows a cold bias during winter as well.

Fig. 4 shows the increment in the T_{\max} averaged for the early (2020–2049), middle (2050–2079), and far (2080–99) future under the RCP-8.5 emission scenario. The changes were calculated with reference to the historical period 1980–2005. It is evident that temperature will rise linearly throughout the country in the 21st century, with more rise in the far future than the near future. The accretion is in the 0.5–2 °C range during the early future, 2–4 °C during the middle future, and 4–6.5 °C during the far future. The maximum increase is observed over

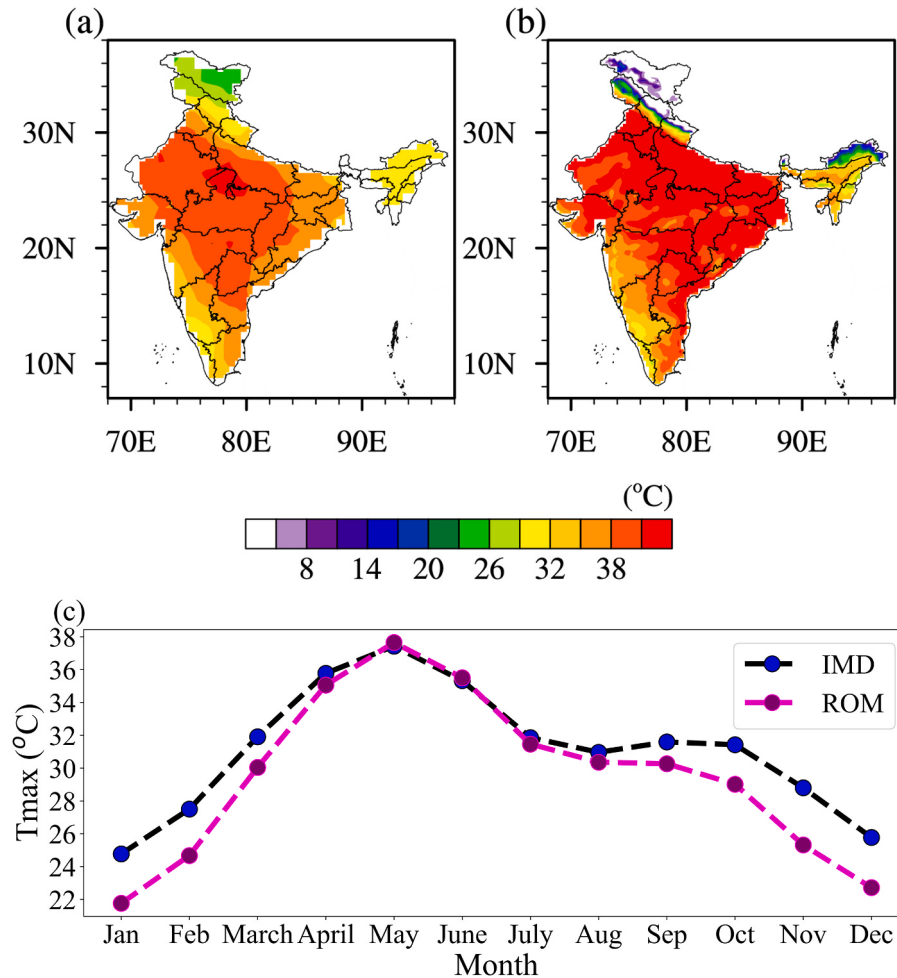


Fig. 3. The spatial distribution of AMJ T_{\max} for (a) IMD, (b) ROM, (c) Annual cycle of area-averaged IMD and ROM for 1980–2005.

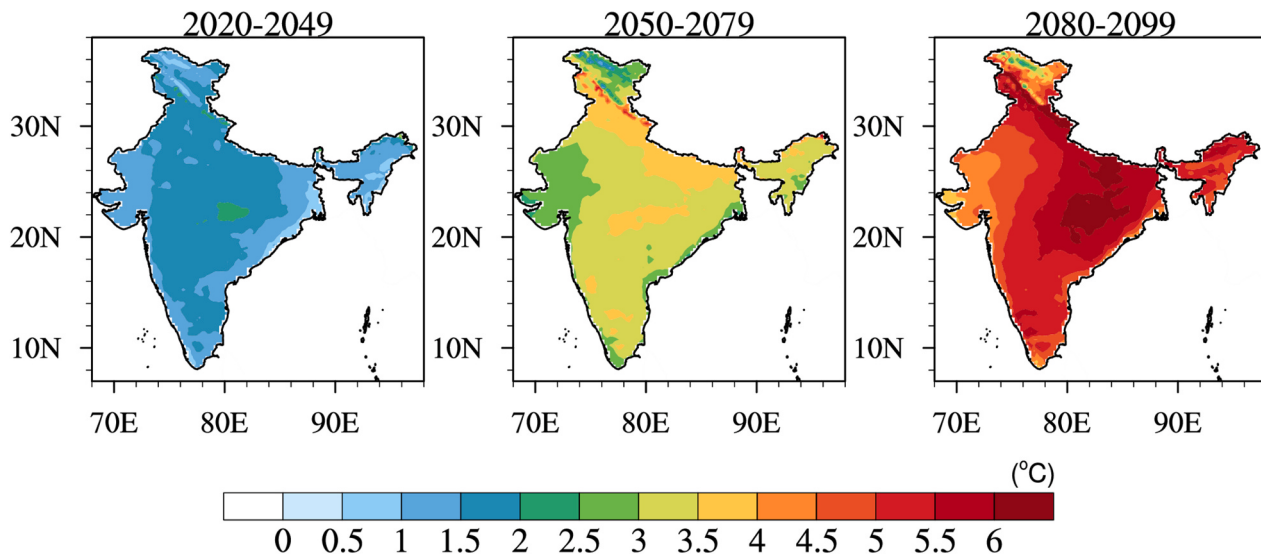


Fig. 4. Future projections of the average AMJ difference in T_{\max} for the early, middle, and far future with respect to 1980–2005.

the east-central and northern regions of India. Most of India's regions are already experiencing heatwave except elevated areas like northeast India and the Himalayas. This regular increase in T_{\max} is responsible for multiple repercussions with an immediate increase in hot temperature days and heatwave events. The associated hazards will also increase in the future.

3.2. Heatwave hazard and risk evaluation

3.2.1. Hazard

The heatwave is considered a hazard due to its catastrophic effect on humans and other organisms. To define heatwave hazard, we considered heatwave frequency as its best proxy for its measurement. Heatwave frequency considers both the magnitude and duration (in terms of length) which can best define the hazard. For future projection, it is necessary to evaluate model skill in capturing the heatwave hazard. The hazard calculated using observation and ROM is shown in Fig. 5. It can be seen that ROM can capture the hazard very efficiently with slight differences over some regions while comparing observations. The most hazardous regions include districts from Malabar coasts, central India,

Indo-Gangetic plains (IGP), and some districts from northwest regions. In contrast, the least affected regions are the northern Himalayas, west coast, and northeast regions. Across India, the western coastal districts have shown the least hazard. ROM simulation results are able to capture the spatial characteristics of hazardous regions very well; however, the magnitude of hazard is less. Out of ~718 districts, the heatwave hazard magnitude over districts in northeast India is different in ROM compared to IMD. It might be due to the opposite behaviour of ROM compared to IMD over northeast India.

3.2.2. Vulnerability

The vulnerability towards any hazard is attributed to the different attributes of populations. Different classes of population have different types of sensitivity towards hazards. Because of this, scarcely populated districts can trigger inaccurate vulnerability estimates. The age and sex of a population cause modification in the heat-health relationship (Basu, 2009; Glass et al., 2015). Infants, elders, and comorbid populations are more vulnerable to heatwave than other age groups (Ding et al., 2016). Similarly, the urban and rural environment, income, and type of household have different exposure on populations and are a

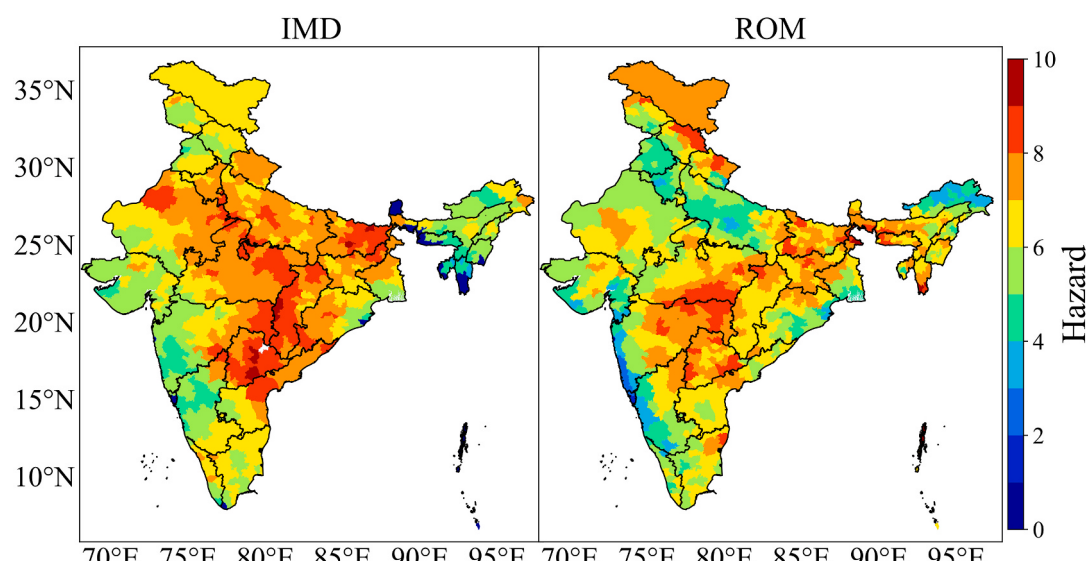


Fig. 5. District wise heatwave hazard map over India for 1980–2005.

determinant factor of vulnerability (Bernhard et al., 2015). Other factors, such as occupation, body size, and economy, also play an essential role in determining the vulnerability of heatwave hazards. Similarly, other population characteristics can contribute to the estimates of vulnerability in both positive and negative ways. Keeping these in the background, we have used twenty-two variable (dimensional) factors (Table S1) that may modify the vulnerability estimates. Demography and socioeconomic data were taken from the year 2011 for the vulnerability analysis.

The heatwave vulnerability based on the census of India dataset is shown in Fig. 6. The higher vulnerable districts are observed in northeast coasts, IGP, and a few districts with metropolitan cities such as Mumbai, Pune, Kolkata, and Bengaluru. This is because of the large population, higher marginal and agricultural workers, illiteracy and lower income (Hajat et al., 2005; Azhar et al., 2017). The districts with metropolitan regions show higher vulnerability mainly due to the higher population, whereas middle IGP shows comparatively lower vulnerability than the districts with mega urban regions despite having a higher population. It might be due to the adaptive ability that makes them relatively less vulnerable. Some of the largest populous cities, such as Mumbai, Delhi, and Kolkata, show the highest vulnerability. The high vulnerability is mainly attributable to the higher illiterate, agricultural and outdoor workers in the populous districts. The hilly and mountainous regions are the least vulnerable as these regions are the least populated.

3.2.3. Risk

The calculated risk is shown in Fig. 7. Risk factors include hazard from IMD and ROM data, exposure and vulnerability from CoI during 1980–2005. It is evident that districts from the southeast coast, northwest and IGP are at higher risk. Among all, the southwest coast (Andhra Pradesh and Telangana) has the greatest exposure to heat due to hot weather. In the northernmost part of India, northeast regions, and the west coast, heatwave risk is not high enough to warrant a warning. Among all, Andhra Pradesh has the highest risk due to heatwaves, followed by the IGP. These regions also observed the highest mortality attributable to heatwaves, with the highest mortality in Andhra Pradesh (Ray et al., 2021). The metropolitan districts of Mumbai, Pune, Delhi and Kolkata also have the highest risk due to higher vulnerability and hazard in these districts. In the northernmost part of India, northeast regions, and west coast, heatwave risk is not enough to cause any

danger. ROM captured the key regions of heatwave risk except for some regions like some districts of Gangetic plains (Uttar Pradesh) and Madhya Pradesh. Despite having biases over IGP in T_{max} , the risk is well captured in ROM. High risk across Andhra Pradesh and Telangana districts is due to high exposure and susceptibility to heatwave hazards. The severity of the risk is 5–8 times higher than in the Himalayan and northeast regions.

3.3. Future projection of heatwave hazard, vulnerability, and risk

The hazard associated with heatwave during the future period is divided into three-time slices: 2020–2049, 2050–2079, and 2080–2099. The mean projected hazard is compared with the base period hazard in the ROM is shown in Fig. 8 (upper panel). It is evident that the heatwave hazard will increase as we head into the future. The hazard scale is almost negligible (0–2) at present and has risen in the range of 2–5 in the early future. The hazard scale rises to 8 in the middle future with maximum hazard over the central Indian and central peninsular region. At the end of the century, the hazard rises to 10. The most hazardous regions have shifted in the northwest, middle and eastern IGP (Orissa and West Bengal), upper northeast (Arunachal Pradesh), northwest and central peninsular regions. It is important to note that some districts in Kerala and northeast regions show a higher level of threat, which was the least affected during the base period.

Similarly, future vulnerability is shown in Fig. 8 (middle panel) using SEDAC population data. It is challenging to get all the population attributes that have been used for the recent period (Table S1). Therefore, we projected a risk based on the future population of SSP4 and heatwave hazard projection using the RCP 8.5 emission scenario and compared it with the base period. The IGP and Kerala districts had a high vulnerability in 2011, which has increased further in the future in all time slices, but the vulnerability by the end of the century is similar to 2080 depicting the stabilization of population after 2080 under the SSP4.

The future risk map based on the above-discussed vulnerability and hazard is illustrated in Fig. 8 (lower panel). Since the risk is the hazard and vulnerability product, the districts having high hazard and vulnerability will have high risk. The future risk has increased gradually from the base period till the end of the century. The time slice 2020–2049 risk is similar to the hazard despite having a more considerable vulnerability over the IGP. At the end of the century, the spatial pattern of risk is maximum over Gangetic plains due to high vulnerability and hazard over the region. Each district of India will be at higher risk of heatwave by the end of the century. Therefore, it will require better planning and adaptation strategies to deal with it, or the emission of greenhouse gases should be reduced so that the levels of warming remain below certain levels such as 1.5° or below. Another aspect will be to keep population growth stabilized or negative so that the appropriate resources can be used to keep the population safe from heatwave hazards. The socio-economic status will play a critical role here, as there are large differences in the high and low-income population's status, and this difference is increasing over time (Deaton and Dreze, 2002; Kurian, 2000; Pieters, 2010).

The projection of future risk is based on considering the population as a vulnerability dimension, and other dimensions such as adaptive capacity, socioeconomic status, migration from rural to urban or vice versa, etc., are not considered. Therefore, the future projection results may be different when these dimensions are considered, but it is evident that the hazard will increase and hence risk. The heatwave has become a global disaster with rising temperatures and further going to accelerate in the future (IPCC, 2014), thereby increasing heat extremes. Even though the countries under the Paris agreement agreed to limit the emission to curb the temperature rise up to 1.5 °C, the climate-related disaster has been increasing. The projection of heatwave-health risk contributes to developing insights to address one of the targets of SDG 13 by adopting appropriate measures for future national policy and planning for heatwave disaster mitigation. Since the heatwave related

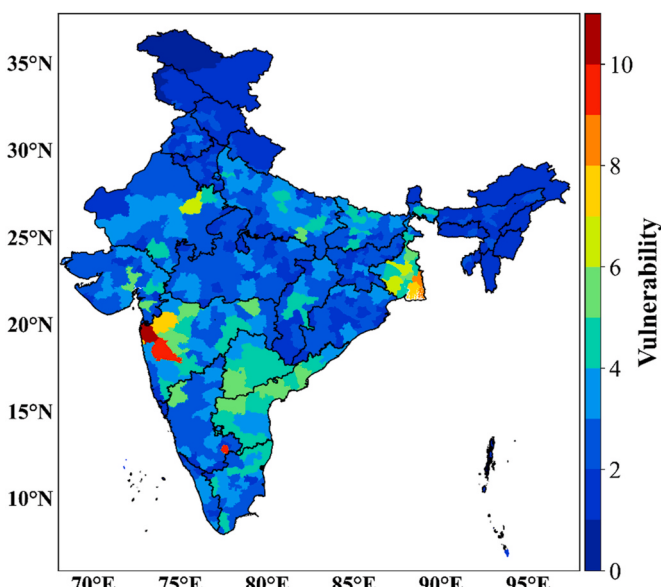


Fig. 6. The vulnerability map of Indian districts using a census of India dataset of 2010.

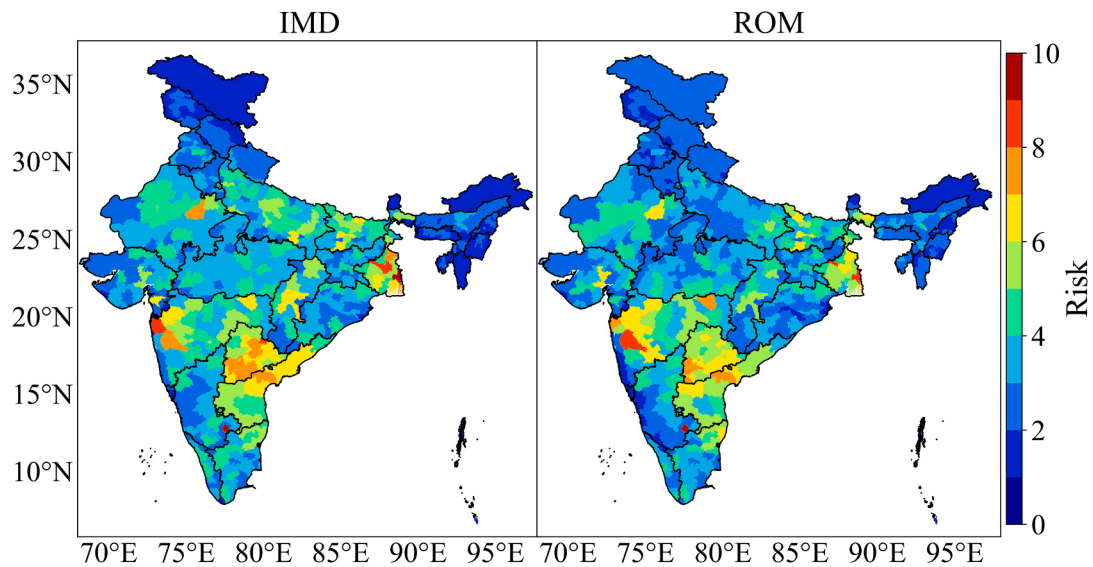


Fig. 7. Risk map generated using hazard from IMD and ROM for 1980–2005 and census of India vulnerability of 2010.

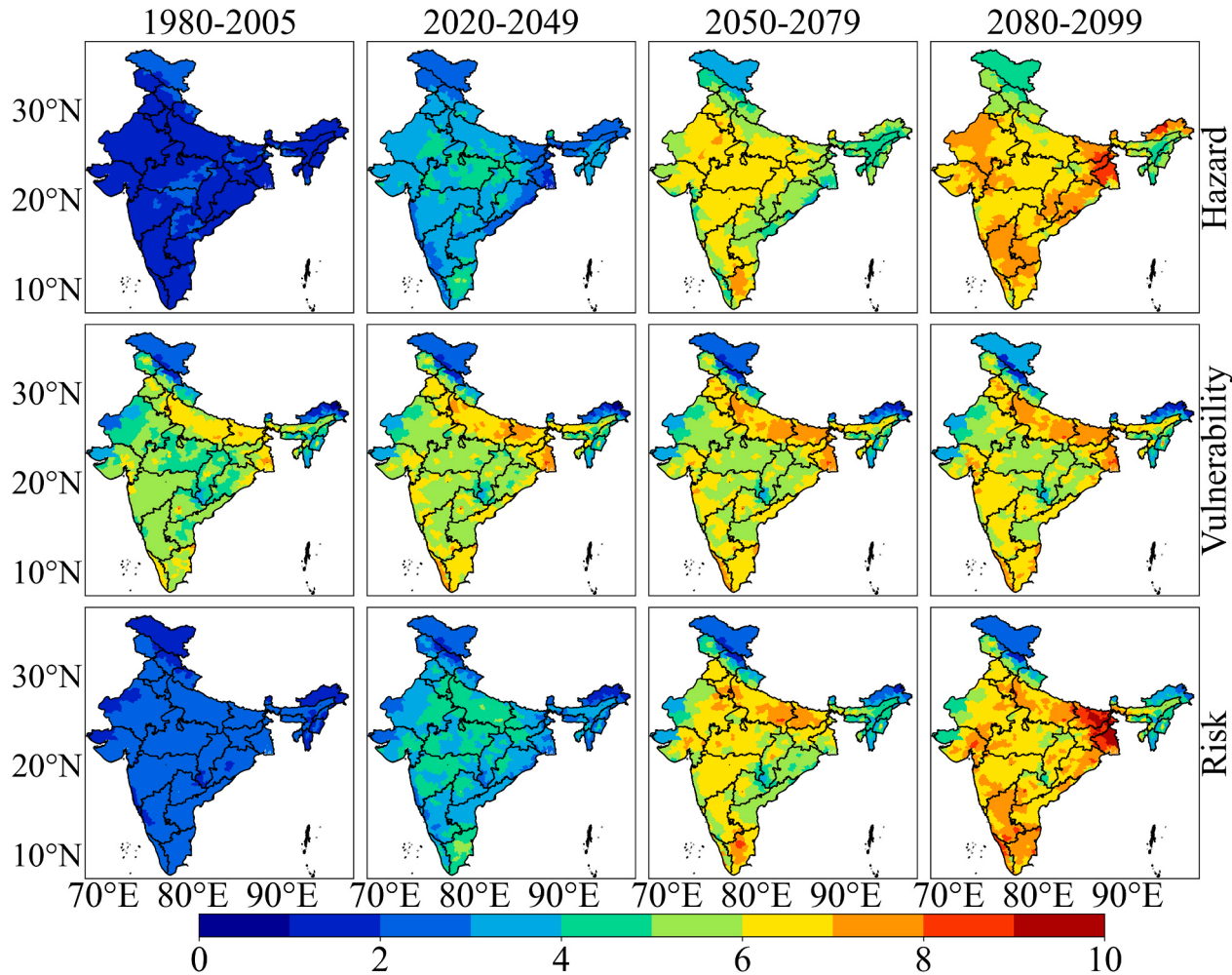


Fig. 8. The maps of future projected Hazard (upper panel), Vulnerability (middle panel), and Risk (lower panel) for the periods 1958–2005 (first column), 2020–2049 (second column), 2050–2079 (third column), and 2080–2099 (fourth column).

mortality/morbidity data is not publicly available, therefore in the future, we would also explore our results with the heatwave related health impacts.

4. Conclusions

The present study highlights the heatwave hazards and risks in

current and future scenarios over India using a coupled regional ocean-atmosphere model ROM and vulnerability using SEDAC projected population data which is the first attempt of its kind. The district-level study for the present scenario demonstrated that the heatwave hazard is high in the southeast coasts, IGP, and northwest regions of India, while the high vulnerability was observed in the northeast coasts, central, eastern IGP, and a few metropolitan regions. The districts primarily with a high hazard as well as high vulnerability had higher heatwave risk. In contrast, districts in the Malabar coast, north-eastern India, and Himalayan regions have very low risk. The ROM model efficiently captured the high hazard regions barring minimal spatial variations, albeit less as compared to the IMD and created high confidence in the ROM model for future simulations.

The ROM model based study demonstrated an increase in the heatwave hazard-risk primarily due to increased temperature under the RCP 8.5 scenario. The hazard increased invariably during each period (2020–2049, 2050–2079, and 2080–99) relative to the base period 1980–2005, with a maximum increase at the end of the century. While future vulnerability increases in the pan India scale irrespective of the geographical variation with a maximum magnitude over IGP. The SSP4 projected population-based heatwave risk exhibited varied estimations compared to risk estimated from CoI socioeconomic datasets. The SDG 13 (climate action) relied on the low Notre Dame Global Adaptation Initiative (ND-GAIN) reported the high vulnerability of the Indian region to climate-related hazards (<https://datatopics.worldbank.org/sdgatlasse/goal-13-climate-action/>). The present study will contribute in determining the high heatwave hazard, vulnerability, and risk zones at district scale over India that can be used to formulate suitable adaptation and mitigation strategies to deal with the present and future heatwave hazard-risk.

Declaration of competing interest

The authors declare that they have no known competing financial interests or personal relationships that could have appeared to influence the work reported in this paper.

Acknowledgement

The first author thanks the Indian Institute of Science Education and Research (IISER) Bhopal, India, for providing a research fellowship. PK acknowledges funding from the Science and Engineering Research Board (SERB), Govt. of India grant numbers SB/S2/RJN-080/2014, and Climate Change Programme-(SPLICE), Department of Science & Technology, India grants number DST/CCP/NCM/69/2017. This work is jointly supported by the Department of Science and Technology (DST), Govt. of India, grant number DST/INT/RUS/RSF/P-33/G, and the Russian Science Foundation (Project No.: 19-47-02015) through a project “Impact of climate change on South Asia extremes: A high-resolution regional Earth System Model assessment”. The observational dataset was downloaded from the Indian Meteorological Department (IMD). AYD worked in the framework of the state assignment of the Ministry of Science and Higher Education of Russia (No 0128-2021- 0014). This work used resources of the Deutsches Klimarechenzentrum (DKRZ) granted by its Scientific Steering Committee (WLA) under project ID ba1144.

Appendix A. Supplementary data

Supplementary data to this article can be found online at <https://doi.org/10.1016/j.envres.2021.111573>.

Data Statement

The IMD maximum temperature data has been downloaded from https://www.imdpune.gov.in/Clim_Pred_LRF_New/Grided_Data_Down

[load.html](#). The demographic dataset has been obtained from the census of India. Future population dataset has been downloaded from <https://sedac.ciesin.columbia.edu/data/collection/gpw-v4>. The earth system model ROM datasets can be obtained upon request from the corresponding author.

Funding information

This work is supported by funding from the Science and Engineering Research Board (SERB), Govt. of India grant numbers SB/S2/RJN-080/2014, Climate Change Programme-(SPLICE), Department of Science & Technology, India grants number DST/CCP/NCM/69/2017, and Department of Science and Technology (DST), Govt. of India, grant number DST/INT/RUS/RSF/P-33/G.

Authors statement

Aditya Kumar Dubey: Conceptualization, Data curation, Formal analysis, Methodology, Software, Visualization, Writing - original draft, Validation Preet Lal: Data curation, Methodology, Software Pankaj Kumar: Conceptualization, Resources, Funding acquisition, Supervision, Writing - review & editing Amit Kumar: Writing - review & editing Anton Y. Dvornikov: Model simulation.

References

- Arakawa, A., Lamb, V.R., 1977. Computational Design of the Basic Dynamical Processes of the UCLA General Circulation Model. Elsevier, pp. 173–265. <https://doi.org/10.1016/b978-0-12-460817-7.50009-4>.
- Azhar, G., Saha, S., Ganguly, P., Mavalankar, D., Madrigano, J., 2017. Heat wave vulnerability mapping for India. Int. J. Environ. Res. Publ. Health 14. <https://doi.org/10.3390/ijerph14040357>.
- Azhar, G.S., Mavalankar, D., Nori-Sarma, A., Rajiva, A., Dutta, P., Jaiswal, A., Sheffield, P., Knowlton, K., Hess, J.J., 2014. Heat-related mortality in India: excess all-cause mortality associated with the 2010 Ahmedabad heat wave. PloS One 9. <https://doi.org/10.1371/journal.pone.0091831>.
- Barriopedro, D., Fischer, E.M., Luterbacher, J., Trigo, R.M., García-Herrera, R., 2011. The hot summer of 2010: redrawing the temperature record map of Europe. Science (80-332), 220–224. <https://doi.org/10.1126/science.1201224>.
- Basarin, B., Lukic, T., Matzarakis, A., 2020. Review of biometeorology of heatwaves and warm extremes in Europe. Atmosphere 11, 1276. <https://doi.org/10.3390/atmos11121276>.
- Basu, R., 2009. High ambient temperature and mortality: a review of epidemiologic studies from 2001 to 2008. Environ. Heal. A Glob. Access Sci. Source 8, 40. <https://doi.org/10.1186/1476-069X-8-40>.
- Bernhard, M.C., Kent, S.T., Sloan, M.E., Evans, M.B., McClure, L.A., Gohlke, J.M., 2015. Measuring personal heat exposure in an urban and rural environment. Environ. Res. 137, 410–418. <https://doi.org/10.1016/j.envres.2014.11.002>.
- Bolin, R., Stanford, L., 1999. Constructing Vulnerability in the First World: the Northridge Earthquake in Southern California, 1994.
- Buscail, C., Upegui, E., Viel, J.F., 2012. Mapping heatwave health risk at the community level for public health action. Int. J. Health Geogr. 11, 1–9. <https://doi.org/10.1186/1476-072X-11-38>.
- Calvin, K., Bond-Lamberty, B., Clarke, L., Edmonds, J., Eom, J., Hartin, C., Kim, S., Kyle, P., Link, R., Moss, R., McJeon, H., Patel, P., Smith, S., Waldhoff, S., Wise, M., 2017. The SSP4: a world of deepening inequality. Global Environ. Change 42, 284–296. <https://doi.org/10.1016/j.gloenvcha.2016.06.010>.
- Clarke, J.F., 1972. Some effects of the urban structure on heat mortality. Environ. Res. 5, 93–104. [https://doi.org/10.1016/0013-9351\(72\)90023-0](https://doi.org/10.1016/0013-9351(72)90023-0).
- Deaton, A., Dreze, J., 2002. Poverty and inequality in India: a re-examination. Econ. Polit. Wkly. 3729–3748.
- Diffenbaugh, N.S., Pal, J.S., Trapp, R.J., Giorgi, F., 2005. Fine-scale processes regulate the response of extreme events to global climate change. Proc. Natl. Acad. Sci. Unit. States Am. 102, 15774–15778. <https://doi.org/10.1073/pnas.0506042102>.
- Ding, Z., Li, L., Xin, L., Pi, F., Dong, W., Wen, Y., Au, W.W., Zhang, Q., 2016. High diurnal temperature range and mortality: effect modification by individual characteristics and mortality causes in a case-only analysis. Sci. Total Environ. 544, 627–634. <https://doi.org/10.1016/j.scitotenv.2015.12.016>.
- Dosio, A., 2016. Projections of climate change indices of temperature and precipitation from an ensemble of bias-adjusted high-resolution EURO-CORDEX regional climate models. J. Geophys. Res. 121, 5488–5511. <https://doi.org/10.1002/2015JD024411>.
- Dubey, A.K., Kumar, P., Saharwardi, M.S., Javed, A., 2021. Understanding the hot season dynamics and variability across India. Weather Clim. Extrem. 32, 100317. <https://doi.org/10.1016/j.wace.2021.100317>.
- Gao, J., 2017. Downscaling global spatial population projections from 1/8-degree to 1-km grid cells. NCAR Technical Note NCAR/TN-537+STR. <https://doi.org/10.5065/D60Z721H>.

- Gao, J., 2020. Global 1-km Downscaled Population Base Year and Projection Grids Based on the Shared Socioeconomic Pathways, Revision 01. Palisades, NY: NASA Socioeconomic Data and Applications Center (SEDAC). <https://doi.org/10.7927/q7z9-9r69>.
- Gao, Y., Weiher, S., Markkanen, T., Pietikäinen, J.P., Gregow, H., Henttonen, H., Jakob, D., Laaksonen, A., 2015. Implementation of the CORINE land use classification in the regional climate model REMO. *Boreal Env. Res.* 261–282.
- Giorgi, F., Coppola, E., Raffaele, F., Diro, G.T., Fuentes-Franco, R., Giuliani, G., Mamgain, A., Llopard, M.P., Mariotti, L., Torma, C., 2014. Changes in extremes and hydroclimatic regimes in the CREMA ensemble projections. *Climatic Change* 125 (1), 39–51. <https://doi.org/10.1007/s10584-014-1117-0>.
- Giorgetta, M.A., Jungclaus, J., Reick, C.H., Legutke, S., Bader, J., Böttger, M., Brovkin, V., Crueger, T., Esch, M., Fieg, K., Glushak, K., Gayler, V., Haak, H., Hollweg, H.-D., Ilyina, T., Kinne, S., Kornblueh, L., Matei, D., Mauritsen, T., Mikolajewicz, U., Mueller, W., Notz, D., Pitman, F., Raddatz, T., Rast, S., Redler, R., Roeckner, E., Schmidt, H., Schnur, R., Segschneider, J., Six, K.D., Stockhausen, M., Timmermann, C., Wegner, J., Widmann, H., Wiemers, K.-H., Claussen, M., Marotzke, J., Stevens, B., 2013. Climate and carbon cycle changes from 1850 to 2100 in MPI-ESM simulations for the Coupled Model Intercomparison Project phase 5. *J. Adv. Model. Earth Syst.* 5, 572–597. <https://doi.org/10.1002/jame.20038>.
- Glass, K., Tait, P.W., Hanna, E.G., Dear, K., 2015. Estimating risks of heat strain by age and sex: a population-level simulation model. *Int. J. Environ. Res. Publ. Health* 12, 5241–5255. <https://doi.org/10.3390/ijerph120505241>.
- Hagemann, S., Dümenil Gates, L., 2001. Validation of the hydrological cycle ECMWF and NCEP reanalyses using the MPI hydrological discharge model. *J. Geophys. Res. Atmos.* 106, 1503–1510. <https://doi.org/10.1029/2000jd900568>.
- Hagemann, S., Göttel, H., Jacob, D., Lorenz, P., Roeckner, E., 2009. Improved regional scale processes reflected in projected hydrological changes over large European catchments. *Clim. Dynam.* 32, 767–781. <https://doi.org/10.1007/s00382-008-0403-9>.
- Hajat, S., Armstrong, B.G., Gouveia, N., Wilkinson, P., 2005. Mortality displacement of heat-related deaths: a comparison of Delhi, São Paulo, and London. *Epidemiology* 16, 613–620. <https://doi.org/10.1097/01.ede.0000164559.41092.2a>.
- Im, E.S., Pal, J.S., Eltahir, E.A.B., 2017. Deadly heat waves projected in the densely populated agricultural regions of South Asia. *Sci. Adv.* 3, e1603322 <https://doi.org/10.1126/sciadv.1603322>.
- IPCC, 2014. Impacts, adaptation, and vulnerability. Part A: global and sectoral aspects. In: Field, C.B., et al. (Eds.), Contribution of Working Group II to the Fifth Assessment Report of the Intergovernmental Panel on Climate Change. Cambridge University Press, Cambridge and New York, USA, pp. 1–32, 2014.
- Jacob, D., Van Den Hurk, B.J.M., Andrae, U., Elgered, G., Fortelius, C., Graham, L.P., Jackson, S.D., Karstens, U., Köcken, C., Lindau, R., Podzun, R., Rockel, B., Rubel, F., Sass, B.H., Smith, R.N.B., Yang, X., 2001. A comprehensive model inter-comparison study investigating the water budget during the BALTEX-PIDCAP period. *Meteorol. Atmos. Phys.* 77, 19–43. <https://doi.org/10.1007/s007030170015>.
- Jungclaus, J.H., Fischer, N., Haak, H., Lohmann, K., Marotzke, J., Matei, D., Mikolajewicz, U., Notz, D., Storch, JS von, 2013. Characteristics of the ocean simulations in the Max Planck Institute Ocean Model (MPIOM) the ocean component of the MPI-Earth system model. *J. Adv. Model. Earth Syst.* 5 (2), 422–446. <https://doi.org/10.1002/jame.20023>.
- KC, S., Lutz, W., 2017. The human core of the shared socioeconomic pathways: population scenarios by age, sex and level of education for all countries to 2100. *Global Environ. Change* 42, 181–192. <https://doi.org/10.1016/j.gloenvcha.2014.06.004>.
- Klinenberg, E., 2003. Review of heat wave: social autopsy of disaster in chicago. *N. Engl. J. Med.* 348, 666–667. <https://doi.org/10.1056/nejm200302133480721>.
- Kumar, P., Wiltshire, A., Mathison, C., Ashraf, S., Ahrens, B., Lucas-Picher, P., Christensen, J.H., Gobiet, A., Saeed, F., Hagemann, S., Jacob, D., 2013. Downscaled climate change projections with uncertainty assessment over India using a high resolution multi-model approach. *Sci. Total Environ.* 468–469. <https://doi.org/10.1016/j.scitotenv.2013.01.051>. S18–S30.
- Kurian, N.J., 2000. Widening regional disparities in India: some indicators. *Econ. Polit. Wkly.* 538–550.
- Maier-Reimer, E., 1993. Geochemical cycles in an ocean general circulation model. Preindustrial tracer distributions. *Global Biogeochem. Cycles* 7, 645–677. <https://doi.org/10.1029/93GB01355>.
- Maier-Reimer, E., Kriest, I., Segschneider, J., Wetzel, P., 2005. The Hamburg Ocean Carbon Cycle Model Hamoccc5. 1-technical Description Release 1.1. Reports on Earth System Science. Max Planck Institute for Meteorolol, Hamburg. <http://edoc.mpg.de/get.epl?fid=1757&did=249293&ver=0>.
- Majewski, D., 1991. The EUROPA-modell of the deutscher wetterdienst. In: Seminar on Numerical Methods in Atmospheric Models, 9–13 September 1991. ECMWF, Reading, pp. 147–193. Shinfield Park.
- Marsland, S.J., Haak, H., Jungclaus, J.H., Latif, M., Röske, F., 2003. The Max-Planck-Institute global ocean/sea ice model with orthogonal curvilinear coordinates. *Ocean Model.* 5 (2), 91–127. [https://doi.org/10.1016/S1463-5003\(02\)00015-X](https://doi.org/10.1016/S1463-5003(02)00015-X).
- McCarthy, J.J., Canziani, O.F., Leary, N.A., Dokken, D.J., White, K.S. (Eds.), 2001. Climate Change 2001: Impacts, Adaptation, and Vulnerability: Contribution of Working Group II to the Third Assessment Report of the Intergovernmental Panel on Climate Change, vol. 2. Cambridge University Press.
- Meehl, G.A., Tebaldi, C., 2004. More intense, more frequent, and longer lasting heat waves in the 21st century. *Science* (80–305), 994–997. <https://doi.org/10.1126/science.1098704>.
- Mishra, A.K., Dwivedi, S., 2019. Assessment of convective parametrization schemes over the Indian subcontinent using a regional climate model. *Theor. Appl. Climatol.* 137, 1747–1764. <https://doi.org/10.1007/s00704-018-2679-y>.
- Mishra, A.K., Dwivedi, S., Das, S., 2020a. Role of Arabian Sea warming on the Indian summer monsoon rainfall in a regional climate model. *Int. J. Climatol.* 40, 2226–2238. <https://doi.org/10.1002/joc.6328>.
- Mishra, A.K., Dwivedi, S., Di Sante, F., 2021a. Performance of the RegCM-MITgcm coupled regional model in simulating the Indian summer monsoon rainfall. *Pure Appl. Geophys.* 1–15. <https://doi.org/10.1007/s0024-020-02648-0>.
- Mishra, A.K., Dwivedi, S., Di Sante, F., Coppola, E., 2020b. Thermodynamical properties associated with the Indian summer monsoon rainfall using a regional climate model. *Theor. Appl. Climatol.* 141, 587–599. <https://doi.org/10.1007/s00704-020-03237-w>.
- Mishra, A.K., Kumar, P., Dubey, A.K., Javed, A., Saharwardi, M.S., Sein, D.V., Martyanov, S.D., Jacob, D., 2021b. Impact of horizontal resolution on monsoon precipitation for CORDEX-South Asia: a regional earth system model assessment. *Atmos. Res.* 259, 105681. <https://doi.org/10.1016/j.atmosres.2021.105681>.
- Mishra, V., Mukherjee, S., Kumar, R., Stone, D.A., 2017. Heat wave exposure in India in current, 1.5 °c, and 2.0 °c worlds. *Environ. Res. Lett.* 12, 124012. <https://doi.org/10.1088/1748-9326/aa9388>.
- Mukherjee, S., Mishra, V., 2018. A sixfold rise in concurrent day and night-time heatwaves in India under 2 °c warming. *Sci. Rep.* 8, 16922. <https://doi.org/10.1038/s41598-018-35348-w>.
- Murari, K.K., Ghosh, S., Patwardhan, A., Daly, E., Salvi, K., 2015. Intensification of future severe heat waves in India and their effect on heat stress and mortality. *Reg. Environ. Change* 15, 569–579. <https://doi.org/10.1007/s10113-014-0660-6>.
- Otto, F.E.L., Massey, N., Van Oldenborgh, G.J., Jones, R.G., Allen, M.R., 2012. Reconciling two approaches to attribution of the 2010 Russian heat wave. *Geophys. Res. Lett.* 39 <https://doi.org/10.1029/2011GL050422>.
- Pattanaik, D.R., Mohapatra, M., Srivastava, A.K., Kumar, A., 2017. Heat wave over India during summer 2015: an assessment of real time extended range forecast. *Meteorol. Atmos. Phys.* 129, 375–393. <https://doi.org/10.1007/s00703-016-0469-6>.
- Perkins, S.E., Alexander, L.V., 2013. On the measurement of heat waves. *J. Clim.* 26, 4500–4517. <https://doi.org/10.1175/JCLI-D-12-00383.1>.
- Perkins-Kirkpatrick, S.E., Lewis, S.C., 2020. Increasing trends in regional heatwaves. *Nat. Commun.* 11, 1–8. <https://doi.org/10.1038/s41467-020-16970-7>.
- Pieters, J., 2010. Growth and inequality in India: analysis of an extended social accounting matrix. *World Dev.* 38, 270–281. <https://doi.org/10.1016/j.worlddev.2009.09.006>.
- Ratnam, J.V., Behera, S.K., Ratna, S.B., Rajeevan, M., Yamagata, T., 2016. Anatomy of Indian heatwaves. *Sci. Rep.* 6, 24395. <https://doi.org/10.1038/srep24395>.
- Ratnam, J.V., Giorgi, F., Kaginalkar, A., Cozzini, S., 2009. Simulation of the Indian monsoon using the RegCM3-ROMS regional coupled model. *Clim. Dynam.* 33, 119–139. <https://doi.org/10.1007/s00382-008-0433-3>.
- Ray, K., Giri, R.K., Ray, S.S., Dimri, A.P., Rajeevan, M., 2021. An assessment of long-term changes in mortalities due to extreme weather events in India: a study of 50 years' data. *Weather Clim. Extrem.* 32, 100315. <https://doi.org/10.1016/j.wace.2021.100315>, 1970–2019.
- Riahi, K., van Vuuren, D.P., Kriegler, E., Edmonds, J., O'Neill, B.C., Fujimori, S., Bauer, N., Calvin, K., Dellink, R., Fricko, O., Lutz, W., Popp, A., Cuadrasma, J.C., KC, S., Leimbach, M., Jiang, L., Kram, T., Rao, S., Emmerling, J., Ebi, K., Hasegawa, T., Havlik, P., Humpenöder, F., Da Silva, L.A., Smith, S., Stehfest, E., Bosetti, V., Eom, J., Gernaert, D., Masui, T., Rogelj, J., Streicher, J., Drouet, L., Krey, V., Luderer, G., Harmsen, M., Takahashi, K., Baumstark, L., Doelman, J.C., Kainuma, M., Klimont, Z., Marangoni, G., Lotze-Campen, H., Obersteiner, M., Tabeau, A., Tavoni, M., 2017. The Shared Socioeconomic Pathways and their energy, land use, and greenhouse gas emissions implications: an overview. *Global Environ. Change* 42, 153–168. <https://doi.org/10.1016/j.gloenvcha.2016.05.009>.
- Robine, J.M., Cheung, S.L.K., Le Roy, S., Van Oyen, H., Griffiths, C., Michel, J.P., Herrmann, F.R., 2008. Death toll exceeded 70,000 in Europe during the summer of 2003. *Comptes Rendus Biol.* 331, 171–178. <https://doi.org/10.1016/j.crvi.2007.12.001>.
- Robinson, P.J., 2001. On the definition of a heat wave. *J. Appl. Meteorol.* 40, 762–775. [https://doi.org/10.1175/1520-0450\(2001\)040<0762:otdoah>2.0.co;2](https://doi.org/10.1175/1520-0450(2001)040<0762:otdoah>2.0.co;2).
- Roeckner, E., Arpe, K., Bengtsson, L., Christoph, M., Claussen, M., Dümenil, L., Esch, M., Giorgi, M., Jungclaus, J., Koenigk, C., Kornblueh, L., Manzini, I., Mikolajewicz, U., Schulzweida, U., 1996. The Atmospheric General Circulation Model ECHAM-4: Model Description and Simulation of Present-Day Climate. Max-Planck-Institut für Meteorologie.
- Roeckner E, Bauml G, Bonaventura L, Brokoff P, Esch M, Giorgi MA, Hagemann M, Kirchner S, Kornblueh I, Manzini LE, Rhodin A, Schlesinger U, Schulzweida U, Tompkins A., 2003. The atmospheric general circulation model ECHAM 5. PART I: Model description. Report / Max-Planck-Institut für Meteorologie, 349.
- Rohini, P., Rajeevan, M., Mukhopadhyay, P., 2019. Future projections of heat waves over India from CMIP5 models. *Clim. Dynam.* 53, 975–988. <https://doi.org/10.1007/s00382-019-04700-9>.
- Rohini, P., Rajeevan, M., Srivastava, A.K., 2016. On the variability and increasing trends of heat waves over India. *Sci. Rep.* 6, 26153. <https://doi.org/10.1038/srep26153>.
- Saaty, T.L., Kearns, K.P., 2014. Analytical Planning: the Organization of System. Elsevier.
- Samala, B.K., C, N., Banerjee, S., Kaginalkar, A., Dalvi, M., 2013. Study of the Indian summer monsoon using WRF-ROMS regional coupled model simulations. *Atmos. Sci. Lett.* 14, 20–27. <https://doi.org/10.1002/asl2.409>.
- Sein, D.V., Mikolajewicz, U., Gröger, M., Fast, I., Cabos, W., Pinto, J.G., Hagemann, S., Semmler, T., Izquierdo, A., Jacob, D., 2015. Regionally coupled atmosphere-ocean-sea ice-marine biogeochemistry model ROM: 1. Description and validation. *J. Adv. Model. Earth Syst.* 7, 268–304. <https://doi.org/10.1002/2014MS000357>.
- Sein, D.V., Gröger, M., Cabos, W., Alvarez-Garcia, F.J., Hagemann, S., Pinto, J.G., Izquierdo, A., de la Vara, A., Koldunov, N.V., Dvornikov, A.Y., Limareva, N., Alekseeva, E., Martinez-Lopez, B., Jacob, D., 2020. Regionally coupled atmosphere-ocean-marine biogeochemistry model ROM: 2. Studying the climate change signal in

- the North Atlantic and Europe. *J. Adv. Model. Earth Syst.* 12, e2019MS001646. <https://doi.org/10.1029/2019MS001646>.
- Simmons, A.J., Burridge, D.M., 1981. An energy and angular-momentum conserving vertical finite-difference scheme and hybrid vertical coordinates. *Mon. Weather Rev.* 109, 758–766. [https://doi.org/10.1175/1520-0493\(1981\)109<0758:AEAAMC>2.0.CO;2](https://doi.org/10.1175/1520-0493(1981)109<0758:AEAAMC>2.0.CO;2).
- Singh, N.P., Byjesh, K., Bantilan, C., 2014. Vulnerability to climate change in semi-arid tropics of India: scouting for holistic approach. In: *Vulnerability of Agriculture, Water and Fisheries to Climate Change: toward Sustainable Adaptation Strategies*. Springer Netherlands, pp. 89–100. https://doi.org/10.1007/978-94-017-8962-2_6.
- Singh, S., Mall, R.K., Singh, N., 2020. Changing spatio-temporal trends of heat wave and severe heat wave events over India: an emerging health hazard. *Int. J. Climatol. joc.* 6814 <https://doi.org/10.1002/joc.6814>.
- Smith, T.T., Zaitchik, B.F., Gohlike, J.M., 2013. Heat waves in the United States: definitions, patterns and trends. *Climatic Change* 118, 811–825. <https://doi.org/10.1007/s10584-012-0659-2>.
- Sharma, A., Sharma, D., Panda, S.K., Dubey, S.K., Pradhan, R.K., 2018. Investigation of temperature and its indices under climate change scenarios over different regions of Rajasthan state in India. *Global Planet. Change* 161, 82–96. <https://doi.org/10.1016/j.gloplacha.2017.12.008>.
- Srivastava, A.K., Rajeevan, M., Kshirsagar, S.R., 2009. Development of a high resolution daily gridded temperature data set (1969–2005) for the Indian region. *Atmos. Sci. Lett.* 10, 249–254. <https://doi.org/10.1002/asl.232>.
- Turner, B.L., Kasperson, R.E., Matsone, P.A., McCarthy, J.J., Corell, R.W., Christensen, L., Eckley, N., Kasperson, J.X., Luers, A., Martello, M.L., Polksy, C., Pulsipher, A., Schiller, A., 2003. A framework for vulnerability analysis in sustainability science. *Proc. Natl. Acad. Sci. U. S. A* 100, 8074–8079. <https://doi.org/10.1073/pnas.1231335100>.
- Wobus, C., Zarakas, C., Malek, P., Sanderson, B., Crimmins, A., Kolian, M., Sarofim, M., Weaver, C.P., 2018. Reframing future risks of extreme heat in the United States. *Earth's Futur* 6, 1323–1335. <https://doi.org/10.1029/2018EF000943>.
- Zhang, X., Alexander, L., Hegerl, G.C., Jones, P., Tank, A.K., Peterson, T.C., Trewin, B., Zwiers, F.W., 2011. Indices for monitoring changes in extremes based on daily temperature and precipitation data. *Wiley Interdiscip. Rev. Clim. Chang.* <https://doi.org/10.1002/wcc.147>.
- Zhu, Q., Liu, T., Lin, H., Xiao, J., Luo, Y., Zeng, W., Zeng, S., Wei, Y., Chu, C., Baum, S., Du, Y., Ma, W., 2014. The spatial distribution of health vulnerability to heat waves in guangdong province, China. *Glob. Health Action* 7, 25051. <https://doi.org/10.3402/gha.v7.25051>.
- Zou, L., Zhou, T., 2013. Can a regional ocean-atmosphere coupled model improve the simulation of the interannual variability of the western North Pacific summer monsoon? *J. Clim.* 26, 2353–2367. <https://doi.org/10.1175/JCLI-D-11-00722.1>.